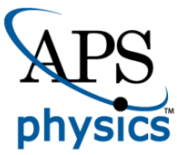

Expansion and retraction dynamics in drop-on-drop impacts on nonwetting surfaces

Maher Damak and Kripa Varanasi

Phys. Rev. Fluids **3**, 093602 — Published 6 September 2018

DOI: 10.1103/PhysRevFluids.3.093602

Expansion and retraction dynamics in drop-on-drop impacts on non-wetting surfaces

Authors: Maher Damak[1], Kripa Varanasi[1*]

Affiliations:

[1]Department of Mechanical Engineering, Massachusetts Institute of Technology. 77 Massachusetts Avenue, Cambridge MA 02139

*Correspondence to: varanasi@mit.edu

Abstract:

Impacts of liquid droplets on other stationary droplets on a surface are ubiquitous in numerous applications such as agricultural sprays, inkjet printing and rain impact on surfaces. We experimentally study the maximum expansion diameter and retraction rate in drop-on-drop impacts on superhydrophobic surfaces. We identify an inertial-capillary and a viscous regime for the expansion phase and we interpret the results using two distinct models. In the inertial-capillary regime, the first model predicts that the maximum diameter is set by an effective capillary length due to the deceleration upon impact. We introduce an effective diameter, velocity and Weber number that allow the accurate determination of the maximum diameter in drop-on-drop impacts. We use our model to predict the transition to the viscous regime and rationalize the maximum diameter in this case with an energy balance. In our second model, we use an energy balance in both regimes and accurately predict the maximum diameter with a unified expression. We finally show that the retraction phase is a no-memory phenomenon and only depends on the volume of the coalesced droplet. We identify capillary and viscous regimes for the retraction and accurately model the retraction rate in each regime. Our approach provides a framework to characterize the dynamics of multiple drop impacts.

I. INTRODUCTION

Drop-on-drop impacts, where a droplet impacts another droplet sitting on a solid surface, are ubiquitous in many applications. In agriculture, when chemicals are sprayed on plants, droplets keep impinging a surface that might be already covered by previous drops, and it is important to know if the liquid will stay on the surface or bounce off and pollute soils and groundwater [1–3]. A recent study showed that by using polyelectrolytes, drop-on-drop impacts can be modified to ensure a substantially larger coverage of the plants [4]. The outcome of sprayed droplets when leaves are covered with dew or rainwater is also of interest [5]. Other major applications are spray painting and thermal sprays where the splat size needs to be carefully controlled [6,7], and inkjet printing where the spreading of the droplets is essential to getting sharp images [8–13]. Predicting the spreading diameter in drop-on-drop impacts can help optimize the spraying or printing parameters. It can also be useful for rapid prototyping [14] and fuel sprays [15]. In other applications, such as icing on airplane wings [16–20] or self-cleaning surfaces [21–23], the quick removal of droplets is advantageous. Determining the retraction rate and contact time of drop-on-drop impacts in these cases can help increase performance and prevent failure.

A few drop-on-drop impact studies have focused on the impact of two droplets, both midair and on a surface, and identified various regimes: coalescence, bouncing and separation after merging [24–31]. For drop-on-drop impacts on a surface, previous studies mostly reported coalescence when the Weber number $We = \frac{\rho D_0 v^2}{\sigma}$ (where ρ is the density of the liquid, σ its surface tension, D_0 the droplet diameter and v the impact speed) is higher than one and we will focus on this case. More recently, the impact of droplets on partially wet surfaces with intermediate hydrophobicity was investigated. The researchers focused on high *We* and identified different fragmentation regimes depending on whether impacts are head-on or offset [32,33]. For head-on impacts on superhydrophobic surfaces, droplets typically expand upon coalescence, reach a

maximum diameter D_{max} and retract, similar to single droplet impacts. Experimental and numerical studies found that for drop-on-drop impacts of water, the maximum diameter follows a $We^{1/4}$ [34] law and the contact time scales as the inertial-capillary time [35] $\tau_i = \left(\frac{\rho R^3}{\sigma}\right)^{1/2}$ [36,37]. These studies however focused on droplets of water of the same size, and the physical mechanism behind this behavior is still largely unexplored.

The impact of a single liquid droplet on a solid surface has been studied much more extensively [18,22,34,38–49]. Upon impact, the droplet similarly undergoes an expansion phase driven by inertia. If the viscosity is low enough, which is the most common case in practice, inertia is balanced by capillary forces until the maximum diameter is reached. Two models have been proposed in the literature to predict this maximum diameter: one relies on an effective capillary length induced by deceleration of the droplet and predicts a diameter varying as $We^{1/4}$ [24] and one using energy conservation at the two limiting cases of negligible viscosity ($D_{max} \sim We^{1/2}$) and high viscosity ($D_{max} \sim Re^{1/5}$) and using an interpolation function between the two [50,51]. Both are successful in predicting the diameter and are used in the literature. For high viscosity flows, viscous forces balance the inertial ones [34,50–53]. If the surface is hydrophobic, a retraction phase follows and the droplet may eventually bounce off the surface. The dynamics are similarly described by an inertial-capillary or a viscous-capillary balance that set the retraction rate [18,35,54].

Here, we systematically study drop-on-drop impacts on a superhydrophobic surface, over a large range of viscosities, impact velocities and droplet sizes. We first focus on the maximum expansion diameter of drop-on-drop impacts in the capillary regime and viscous regimes. We adapt both models used in the literature for single drop impacts to the case of drop-on-drop impacts and show that both can be used successfully. We then investigate the retraction phase. We elucidate the dynamics of the impact and the role of the stationary droplet and develop a generalized model that covers both single and multiple-drop impacts.

II. MATERIALS AND METHODS

The experimental setup we use is shown in Fig. 1(a). A syringe is filled with the fluid of interest and connected to a dispensing needle. The height of the needle is adjusted to control the droplet impact velocity. A second droplet is deposited on the surface directly under the dispensing needle and serves as a stationary droplet. The needles' diameters were varied to change the size of the generated droplets so that the ratio of the impinging to the stationary droplet size was varied. The impact of these droplets was filmed using a high-speed camera (Photron S1) at 10,000 frames per second, with back lighting. High-speed movies were used to measure droplet size (error<3%) and impact velocity (error<1%) resulting in an error of less than 5% for the Weber number. They were also used to measure retraction speed with an error estimated at 10%. More detailed error analysis is in Supplemental Material [56]. We varied the viscosity of the fluid by using water-glycerol mixtures at different ratios, spanning the whole range from pure water ($\sim 10^{-3} Pa.s$) to pure glycerol ($\sim 1.4\ Pa.s$). The surface tension in these mixtures did not vary much and remained between $72 mN/m$ (water) and $64 mN/m$ (glycerol). The surface on which the drop-on-drop impacts were performed is a superhydrophobic surface (Inset of Fig. 1(a)). It was fabricated by making a nanograss silicon surface, with a roughness on the order of 200nm, through reactive ion etching. The surface was then coated with a hydrophobic modifier (Octadecyltrichlorosilane) to reach a contact angle of 165˚ and a contact angle hysteresis of less than 5˚ [55].

III. RESULTS AND DISCUSSION

The typical phases of a drop-on-drop impact are shown schematically in Fig. 1(b) and experimentally in Figs. 1(c) and (d). As an impacting droplet of diameter D_i impinges with a velocity v on a second droplet of diameter D_s sitting on the surface, the droplets merge and start expanding. Depending on the impact speed and viscosity, the expanded droplet may have a donut shape (Fig. 1(c)), where there is a rim of higher thickness than

the center of the droplet, or a pancake shape (Fig. 1(d)), where the thickness is approximately uniform across the radius of the droplet. The former usually occurs for higher impacting speeds and lower viscosities. After the maximum diameter D_{max} is reached, the droplet may retract and bounce if the viscosity is low (Fig. 1(c)). If the viscosity is large, the retraction phase is limited and no bouncing occurs (Fig. 1(d)).

A. The expansion phase

The expansion phase starts with the coalescence of the two droplets. In the inertial-capillary regime (low viscosity), an expanding liquid sheet forms between the droplets and moves downwards (Fig. 1(c)). By the end of the expansion phase, the droplet takes the usual donut shape observed in single drop impacts. We performed experiments with different droplet size ratios in this regime. Figure 2(a) shows snapshots of the impact of a small droplet on a bigger one and the impact of big droplet on a smaller one. The overall phases are the same: the droplet still expands, retracts and bounces off.

To rationalize the expansion behavior in this inertial-capillary regime and to understand the role of the stationary droplet in the process, we first adapt the single droplet impact argument used by Clanet et. al. [34].

At its maximal expansion, the combined droplet looks like a puddle. For a puddle on a flat surface, the shape is dictated by a balance between gravity and surface tension forces. In the case of a drop impact, the droplet attains this shape because it is experiencing an effective gravity field resulting from the deceleration of the impacting drop, which overcomes surface tension and deforms the droplet away from its spherical shape (as puddles form when gravity overcome surface tension) [34]. The thickness of the expanded drop should then scale as the capillary length $h \sim \sqrt{\frac{\sigma}{\rho g^*}}$, where g^* is the vertical acceleration felt by the droplet. In a drop-on-drop impact, the thickness of the combined droplet at maximum expansion is dictated by the deceleration felt by the total volume of the combined droplet. This combined droplet is formed by the impacting droplet, which has a velocity U_0, and the stationary droplet, which is at rest. When the two droplets coalesce, the combined droplet has a diameter $D_t = (D_i^3 + D_s^3)^{1/3}$. At impact, the

momentum of the impacting droplet is $m_i U_0$, where m_i is the mass of the impacting drop. Upon coalescence, the momentum is conserved but the mass of liquid that is moving downwards becomes $m_i + m_s$. Thereby, by momentum conservation, the velocity U_0' of the center of mass of the combined droplet is given by $(m_i + m_s)U_0' = m_i U_0$. The thickness of the expanded combined droplet is governed by the deceleration of this combined droplet from U_0' to 0 over a distance $D_t - h$. The resulting acceleration scales as $g^* \sim \frac{{U_0'}^2}{D_t - h}$.

The thickness of the expanded droplet is then

$$h \sim \sqrt{\frac{\sigma}{\rho g^*}} \sim \sqrt{\frac{\sigma}{\rho {U_0'}^2}(D_t - h)}$$

This equation can be solved for h.

$$h \sim \frac{\sigma}{2\rho {U_0'}^2}\left(\sqrt{1 + \frac{4\rho {U_0'}^2 D_t}{\sigma}} - 1\right) = \frac{D_t}{2We'}\left(\sqrt{1 + 4We'} - 1\right) \qquad (1)$$

where $We' = \frac{\rho {U_0'}^2 D_t}{\sigma}$

We conducted drop-on-drop impacts with various diameter ratios, impact velocities and viscosities and measured the thickness of the combined droplet at maximum expansion. We plot in Fig. 2(b) the theoretical thickness given by the above formula against the experimental thickness. The agreement between theory and experimental results is good and shows that the model captures the dynamics of expansion in drop-on-drop impacts.

Using mass conservation and assuming a pancake shape for the expanded droplet, the maximum diameter can be obtained as

$$\frac{\pi}{4} h D_{max}^2 = \frac{\pi}{6}(D_i^3 + D_s^3) = \frac{\pi}{6} D_t^3$$

and using the expression (1) for h

$$\frac{D_{max}}{D_t} = \sqrt{\frac{2}{3}}\sqrt{\frac{2We'}{\sqrt{1+4We'}-1}} \tag{2}$$

where the modified Weber number is

$$We' = \frac{\sigma U_0^2 (D_i^3 + D_s^3)^{1/3}}{\rho}\left(\frac{m_i}{m_i + m_s}\right)^2 \tag{3}$$

We compare the maximum diameter predicted by our model to experimental measurements in various cases and find good agreement shown in Fig. 2(c).

As shown in the case of single drop impacts, this model is only valid when the size of the combined droplet is larger than the effective capillary length $D_t > \sqrt{\frac{\sigma}{\rho U_0'^2} D_t}$ or $We' > 1$, which is the condition to form a puddle instead of a sphere.

Another condition for the model to be valid is that the deceleration time $\frac{D_t}{U_0'}$ is smaller than the contact time $\sqrt{\frac{\rho}{\sigma} {D_t}^3}$, which also leads to the same criterion $We' > 1$.

One limiting case of this model is the impact of a droplet on a much bigger one $D_i \ll D_s$. Intuitively, if the impact velocity is not too high ($We' \ll 1$), the stationary droplet should barely deform. The expression for D_{max} is not valid here because mass conservation using a pancake shape is not accurate in the low Weber number regime.

However, the expression for *h* remains valid, and in the limit of low We', we recover that the thickness of the combined droplet is the combined diameter, since no deformation would occur and the combined droplet would maintain its spherical shape.

$$h = \frac{D_t}{2We'}\left(\sqrt{1+4We'}-1\right) \sim \frac{D_t}{2We'}(1+2We'-1) = D_t$$

The other limiting case is the impact of a droplet on a much smaller one $D_i \gg D_s$. Intuitively, this case should tend toward single drop impacts. The modified Weber here tends toward the single drop Weber number $We' = \frac{\sigma U_0^2 (D_i^3 + D_s^3)^{1/3}}{\rho}\left(\frac{m_i}{m_i + m_s}\right)^2 \sim \frac{\sigma U_0^2 D_i}{\rho} =$

We and when $We' \gg 1$, $\frac{D_{max}}{D_t} = \sqrt{\frac{2}{3}}\sqrt{\frac{2We'}{\sqrt{1+4We'}-1}} \sim \sqrt{\frac{2}{3}}We'^{1/4}(1+\frac{1}{4\sqrt{We'}}) \sim \sqrt{\frac{2}{3}}We^{1/4}$, which is indeed the scaling law governing single drop impacts [22]. The next order error term that has been neglected here results in a deviation of 25% for $We' = 1$ and the deviation is less than 5% for $We' > 25$.

To further confirm this simplified scaling for the data where $We' > 1$, we plotted $\frac{D_{max}}{D_0}Re^{1/5}$ in Fig. 3 as a function of the impact parameter $P = \frac{We'}{Re^{4/5}}$ over four orders of magnitude of *P*, consistent with literature. In the literature, *P* was used to determine the transition between the inertial and viscous regimes. We see that the data for drop-on-drop and single drop impacts collapses in a single master curve ($Re = \frac{\rho D_t v}{\mu}$ is the Reynolds number). For low *P* (inertial-capillary regime), we observe the classical $\frac{D_{max}}{D_t} \sim We'^{1/4}$ law, whereas for $P > 1$, we transition to a viscous regime.

To rationalize the behavior in this viscous regime, we balance the kinetic energy of the impacting droplet $E_k \sim \rho D_i^3 V^2 \sim \frac{1}{2}\rho D_t^3 V^2$, for droplets of the same size, with the viscous energy dissipation during the expansion phase $E_{visc} = \tau_{visc} A D_{max}$ where $\tau_{visc} \sim \mu \frac{V}{h}$ is the viscous stress, $A \sim D_{max}^2$ is the area on which the stress is applied and D_{max} is the distance over which viscous dissipation occurs [34].

This leads to $E_{visc} = \mu \frac{V}{h} D_{max}^3$, and with volume conservation $hD_{max}^2 \sim D_t^3$ we have

$$\mu \frac{V}{D_t^3} D_{max}^5 \sim \frac{1}{2}\rho D_t^3 V^2$$

which is equivalent to

$$\frac{D_{max}}{D_t} \sim \left(\frac{\rho V D_t}{2\mu}\right)^{1/5} \sim Re^{1/5}$$

We see in Fig. 3 that, indeed, for high *P*, this scaling law predicts the diameter of both drop-on-drop as well as single drop impacts.

The transition from the inertial-capillary to the viscous regime happens when viscous forces become more limiting than capillary forces and thus when the predicted diameter

in the viscous regime becomes smaller than the predicted diameter in the inertial-capillary regime, i.e. when $We'^{1/4} \sim Re^{1/5}$ or $P = \frac{We'}{Re^{4/5}} \sim 1$.

An alternate model for the expansion phase in single drop impacts has been proposed recently to reconcile the energy approach in both the viscous and capillary regimes [50,51]. We showed above that for the viscous regime, an energy approach gives the $Re^{1/5}$ law, both for drop-on-drop and single drop impacts. For single droplets in the capillary regime, if we assume that all the kinetic energy is converted into surface energy in the expanded droplet, we find a $We^{1/2}$ law for the expansion diameter of single drop impacts at high Weber numbers ($\rho D^3 U^2 \sim \sigma D_{max}^2$). Since the observations in most experiments do not follow a $We^{1/2}$ law, it was assumed that most common experiments were in a crossover regime between these viscous and capillary regimes. An interpolation function, based on a Padé approximant, with one free parameter was defined: $D_{max}/D_0 = f(We, Re) = \frac{We^{1/2}}{A + We^{1/2} Re^{-1/5}}$, where A is a fitting constant (equal to 1.24 for single drop impacts) [50]. This function tends to $We^{1/2}$ in the capillary regime and $Re^{1/5}$ in the viscous regime and was shown to predict accurately the maximum expansion diameter.
In the case of drop-on-drop impacts, energy conservation for negligible viscous dissipation gives:

$$\rho D_i^3 U_i^2 + \sigma D_s^2 \sim \sigma D_{max}^2$$

The final surface energy comes from both the kinetic energy of the impacting droplet as well as the surface energy of the stationary droplet.
Thus

$$\frac{\sqrt{D_{max}^2 - D_s^2}}{D_i} \sim We_i^{1/2}$$

where $We_i^{1/2}$ is the Weber number of the impacting droplet.

We similarly define an interpolation function for drop-on-drop impacts that approximates the maximal diameter between the two limiting cases where the initial kinetic energy is either entirely converted to surface energy or entirely dissipated by viscosity.

$$\frac{\sqrt{D_{max}^2 - D_s^2}}{D_i} \sim \frac{We_i^{1/2}}{B + We_i^{1/2} Re^{-1/5}}$$

We find that this function accurately predicts the maximum expansion diameter across the range of our experiments for B=2. The results are shown in Fig. 4
Therefore, both models can be used to predict the maximum expansion diameter. The first model is based on the effective capillary length and mass conservation, while the second model uses energy conservation. Both models accurately predict the maximum diameter for our experimental data (with a similar coefficient of determination R2) similar to what was found in the literature for single drop impacts. While there is still debate in the literature on which of these models, if either, gives the exact formula for single drop impacts, the results presented here show how that model can be translated to drop-on-drop impacts.

B. The retraction phase

Finally, the retraction phase was quantified using the retraction rate $\dot{\varepsilon} = \frac{V_{ret}}{D_{max}}$ where V_{ret} is the retraction speed of the contact line and was measured by image analysis of the high-speed movies. The retraction rate was measured over four orders of magnitude of the Ohnesorge number $Oh = \frac{\mu}{\sqrt{\rho \sigma R}}$, for various droplet size ratios: small on big droplet, same size and big on small droplet. In Fig. 5(a), we plot $\dot{\varepsilon}\tau_i$ as a function of Oh, following what has been done in literature [54], where we use an effective inertial-capillary time $\tau_i = \left(\frac{\rho(R_i^3 + R_s^3)}{\sigma}\right)^{1/2}$. For low Oh, we find that the retraction rate does not depend on the impact velocity and scales as the inverse of the inertial-capillary timescale, confirming and generalizing what was observed before for water drop-on-drop impacts [37]. This scaling does not change when viscosity is modified, as long as the droplet is in the inertial-capillary regime. When $Oh \sim 0.5$, the behavior changes and we enter the viscous regime. The slope of the curve in log-log scale is -1, which means that

the retraction rate scales as the inverse of the viscous-capillary timescale $\tau_v = \frac{\mu(R_i^3+R_s^3)^{1/3}}{\sigma}$, similar to was previously observed for single drop impacts. As can be seen in Fig. 5(a), the retraction rate does not depend on the size ratio, as long as the coalesced size is the same. Figures 5(b) and 5(c) show a drop-on-drop impact with two droplets of the same size and a single droplet impact with a droplet whose size is the same as the two previous droplets combined. The impact velocities were chosen so that both reach the same maximum diameter, and we can see that the retraction dynamics are exactly the same: both droplets retract at the same rate and bounce off at the same time. Figure 5(d) shows a drop-on-drop impact with the same coalesced droplet size but a lower impact velocity. The maximum expansion diameter is smaller here, but the retraction rate is still the same and this droplet also bounces off at the exact same time as the previous two. The explanation for this behavior is that, after the expansion phase, and as the two droplets merge together, the coalesced droplet "forgets" that it was formed by a drop-on-drop impact. The phenomenon has no memory, and it is not possible to retrace the history of the impact just by observing the retraction phase. Thereby, we can adapt the previous models shown for single drop impacts to drop-on-drop impact, by using the coalesced radius as the typical length scale.

IV. CONCLUSION

In this work, we characterized both the expansion and retraction phases of drop-on-drop impacts on superhydrophobic surfaces and established generalized models to describe them. For the maximum droplet expansion, we first developed a model based on effective gravity fields for drop-on-drop impacts encompassing the previously shown model for single drop impacts as a particular case, and we found excellent agreement with experiments. We then adapted another model from the literature that used energy conservation to predict the diameter and found it also gives good agreement with the experimental results. For the retraction rate, we showed that the phenomenon of drop-on-drop impact has no memory and that, after coalescence, the droplet behaves as predicted with single drop models. More generally, our results show that the extensive literature

results on single droplet impacts could be extended and generalized to impacts involving multiple droplets.

In many spray applications, single small droplets impacting a surface will stick, but it is the behavior of subsequent droplets impacting those initial ones that will dictate the liquid expansion, coverage and ultimately the quality of the resulting surface. The models developed here will help precisely control the spreading of ink-jet droplets impacting on each other, get a uniform coverage in spray painting or thermal sprays and accurately choose the parameters in agricultural sprays to make chemicals stick on hydrophobic leaves.

References

[1] M. Massinon and F. Lebeau, Comparison of spray retention on synthetic superhydrophobic surface with retention on outdoor grown wheat leaves, Int. Adv. Pestic. Appl. Asp. Appl. Biol. 114 2012 (2012).

[2] R. J. Gilliom, J. E. Barbash, C. G. Crawford, P. A. Hamilton, J. D. Martin, N. Nakagaki, L. H. Nowell, J. C. Scott, P. E. Stackelberg, and G. P. Thelin, *Pesticides in the Nation's Streams and Ground Water, 1992-2001* (Geological Survey (US), 2006).

[3] V. Bergeron, D. Bonn, J. Y. Martin, and L. Vovelle, Controlling droplet deposition with polymer additives, Nature **405**, 772 (2000).

[4] M. Damak, S. R. Mahmoudi, M. N. Hyder, and K. K. Varanasi, Enhancing droplet deposition through *in-situ* precipitation, Nat. Commun. **7**, (2016).

[5] G. S. Watson, M. Gellender, and J. A. Watson, Self-propulsion of dew drops on lotus leaves: a potential mechanism for self cleaning, Biofouling **30**, 427 (2014).

[6] R. Dhiman, A. G. McDonald, and S. Chandra, Predicting splat morphology in a thermal spray process, Surf. Coatings Technol. **201**, 7789 (2007).

[7] S. D. Aziz and S. Chandra, Impact, recoil and splashing of molten metal droplets, Int. J. Heat Mass Transf. **43**, 2841 (2000).

[8] H. Wijshoff, The dynamics of the piezo inkjet printhead operation, Phys. Reports **491**, 77 (2010).

[9] J. Z. Wang, Z. H. Zheng, H. W. Li, W. T. S. Huck, and H. Sirringhaus, Dewetting of conducting polymer inkjet droplets on patterned surfaces, Nat. Mater. **3**, 171 (2004).
[10] D. Soltman and V. Subramanian, Inkjet-printed line morphologies and temperature control of the coffee ring effect, Langmuir **24**, 2224 (2008).
[11] J. Stringer and B. Derby, Limits to feature size and resolution in ink jet printing, J. Eur. Ceram. Soc. **29**, 913 (2009).
[12] F. Gao and A. A. Sonin, Precise deposition of molten microdrops: the physics of digital microfabrication, Proc R Soc Lond A **444**, 533 (1994).
[13] R. Li, N. Ashgriz, S. Chandra, J. R. Andrews, and J. Williams, Drawback during deposition of overlapping molten wax droplets, J. Manuf. Sci. Eng. **130**, 041011 (2008).
[14] Y. Zhang, Y. Chen, P. Li, and A. T. Male, Weld deposition-based rapid prototyping: a preliminary study, J. Mater. Process. Technol. **135**, 347 (2003).
[15] A. L. N. Moreira, A. S. Moita, and M. R. Panao, Advances and challenges in explaining fuel spray impingement: How much of single droplet impact research is useful?, Prog. Energy Combust. Sci. **36**, 554 (2010).
[16] J. Lv, Y. Song, L. Jiang, and J. Wang, Bio-Inspired Strategies for Anti-Icing, ACS Nano **8**, 3152 (2014).
[17] T. Maitra, M. K. Tiwari, C. Antonini, P. Schoch, S. Jung, P. Eberle, and D. Poulikakos, On the Nanoengineering of Superhydrophobic and Impalement Resistant Surface Textures below the Freezing Temperature, Nano Lett. **14**, 172 (2013).
[18] J. C. Bird, R. Dhiman, H.-M. Kwon, and K. K. Varanasi, Reducing the contact time of a bouncing drop, Nature **503**, 385 (2013).
[19] Y. Boluk, Adhesion of Freezing Precipitates to Aircraft Surfaces, Transp. Can. (1996).
[20] C. C. Ryerson, Ice protection of offshore platforms, Cold Reg. Sci. Technol. **65**, 97 (2011).
[21] R. Blossey, Self-cleaning surfaces — virtual realities, Nat. Mater. **2**, 301 (2003).
[22] A. Lafuma and D. Quéré, Superhydrophobic states, Nat. Mater. **2**, 457 (2003).
[23] X. Deng, L. Mammen, Y. Zhao, P. Lellig, K. Müllen, C. Li, H.-J. Butt, and D. Vollmer, Transparent, Thermally Stable and Mechanically Robust Superhydrophobic Surfaces Made from Porous Silica Capsules, Adv. Mater. **23**, 2962 (2011).
[24] N. Ashgriz, *Handbook of Atomization and Sprays: Theory and Applications* (Springer Science & Business Media, 2011).
[25] F.-C. Wang, J.-T. Feng, and Y.-P. Zhao, The head-on colliding process of binary liquid droplets at low velocity: High-speed photography experiments and modeling, J. Colloid Interface Sci. **326**, 196 (2008).
[26] I. V. Roisman, Dynamics of inertia dominated binary drop collisions, Phys. Fluids **16**, 3438 (2004).
[27] I. V. Roisman, C. Planchette, E. Lorenceau, and G. Brenn, Binary collisions of drops of immiscible liquids, J. Fluid Mech. **690**, 512 (2012).
[28] N. Yi, B. Huang, L. Dong, X. Quan, F. Hong, P. Tao, C. Song, W. Shang, and T. Deng, Temperature-Induced Coalescence of Colliding Binary Droplets on Superhydrophobic Surface, Sci. Reports **4**, (2014).

[29] I. V. Roisman, B. Prunet-Foch, C. Tropea, and M. Vignes-Adler, Multiple drop impact onto a dry solid substrate, J. Colloid Interface Sci. **256**, 396 (2002).
[30] G. Liang and I. Mudawar, Review of mass and momentum interactions during drop impact on a liquid film, Int. J. Heat Mass Transf. **101**, 577 (2016).
[31] A. B. Thompson, C. R. Tipton, A. Juel, A. L. Hazel, and M. Dowling, Sequential deposition of overlapping droplets to form a liquid line, J. Fluid Mech. **761**, 261 (2014).
[32] Y. Wang and L. Bourouiba, Non-isolated drop impact on surfaces, J. Fluid Mech. **835**, 24 (2018).
[33] T. Gilet and L. Bourouiba, Rain-Induced Ejection of Pathogens from Leaves: Revisiting the Hypothesis of Splash-on-Film Using High-Speed Visualization, The Society for Integrative and Comparative Biology, 2014.
[34] C. Clanet, C. Béguin, D. Richard, and D. Quéré, Maximal deformation of an impacting drop, J. Fluid Mech. **517**, 199 (2004).
[35] D. Richard, C. Clanet, and D. Quéré, Surface phenomena: Contact time of a bouncing drop, Nature **417**, 811 (2002).
[36] P. J. Graham, M. M. Farhangi, and A. Dolatabadi, Dynamics of droplet coalescence in response to increasing hydrophobicity, Phys. Fluids 1994-Present **24**, 112105 (2012).
[37] M. M. Farhangi, P. J. Graham, N. R. Choudhury, and A. Dolatabadi, Induced Detachment of Coalescing Droplets on Superhydrophobic Surfaces, Langmuir **28**, 1290 (2012).
[38] D. Quéré, Non-sticking drops, Reports Prog. Phys. **68**, 2495 (2005).
[39] D. Richard and D. Quéré, Bouncing water drops, EPL Eur. Lett. **50**, 769 (2000).
[40] M. Rein, Phenomena of liquid drop impact on solid and liquid surfaces, Fluid Dyn. Res. **12**, 61 (1993).
[41] P.-G. De Gennes, F. Brochard-Wyart, and D. Quéré, *Capillarity and Wetting Phenomena: Drops, Bubbles, Pearls, Waves* (Springer, 2004).
[42] Y. Liu, L. Moevius, X. Xu, T. Qian, J. M. Yeomans, and Z. Wang, Pancake bouncing on superhydrophobic surfaces, Nat. Phys. (2014).
[43] U. Mock, T. Michel, C. Tropea, I. Roisman, and J. Rühe, Drop impact on chemically structured arrays, J. Phys. Condens. Matter **17**, S595 (2005).
[44] X. Deng, F. Schellenberger, P. Papadopoulos, D. Vollmer, and H.-J. Butt, Liquid Drops Impacting Superamphiphobic Coatings, Langmuir **29**, 7847 (2013).
[45] C. Duez, C. Ybert, C. Clanet, and L. Bocquet, Making a splash with water repellency, Nat. Phys. **3**, 180 (2007).
[46] J. de Ruiter, J. M. Oh, D. van den Ende, and F. Mugele, Dynamics of Collapse of Air Films in Drop Impact, Phys. Rev. Lett. **108**, 074505 (2012).
[47] L. Bocquet and E. Lauga, A smooth future?, Nat. Mater. **10**, 334 (2011).
[48] C. Antonini, I. Bernagozzi, S. Jung, D. Poulikakos, and M. Marengo, Water Drops Dancing on Ice: How Sublimation Leads to Drop Rebound, Phys. Rev. Lett. **111**, 014501 (2013).
[49] C. Josserand and S. T. Thoroddsen, Drop Impact on a Solid Surface, Annu. Rev. Fluid Mech. **48**, 365 (2016).
[50] N. Laan, K. G. de Bruin, D. Bartolo, C. Josserand, and D. Bonn, Maximum Diameter of Impacting Liquid Droplets, Phys. Rev. Appl. **2**, 044018 (2014).

[51] J. B. Lee, N. Laan, K. G. de Bruin, G. Skantzaris, N. Shahidzadeh, D. Derome, J. Carmeliet, and D. Bonn, Universal rescaling of drop impact on smooth and rough surfaces, J. Fluid Mech. **786**, R4 (2015).
[52] J. Madejski, Solidification of droplets on a cold surface, Int. J. Heat Mass Transf. **19**, 1009 (1976).
[53] I. V. Roisman, R. Rioboo, and C. Tropea, Normal impact of a liquid drop on a dry surface: model for spreading and receding, Proc. R. Soc. Lond. Math. Phys. Eng. Sci. (The Royal Society, 2002), pp. 1411–1430.
[54] D. Bartolo, C. Josserand, and D. Bonn, Retraction dynamics of aqueous drops upon impact on non-wetting surfaces, J. Fluid Mech. **545**, 329 (2005).
[55] S. Anand, A. T. Paxson, R. Dhiman, J. D. Smith, and K. K. Varanasi, Enhanced Condensation on Lubricant-Impregnated Nanotextured Surfaces, Acs Nano **6**, 10122 (2012).
[56] See Supplemental Material at [] for error analysis and videos of drop-on-drop impacts.

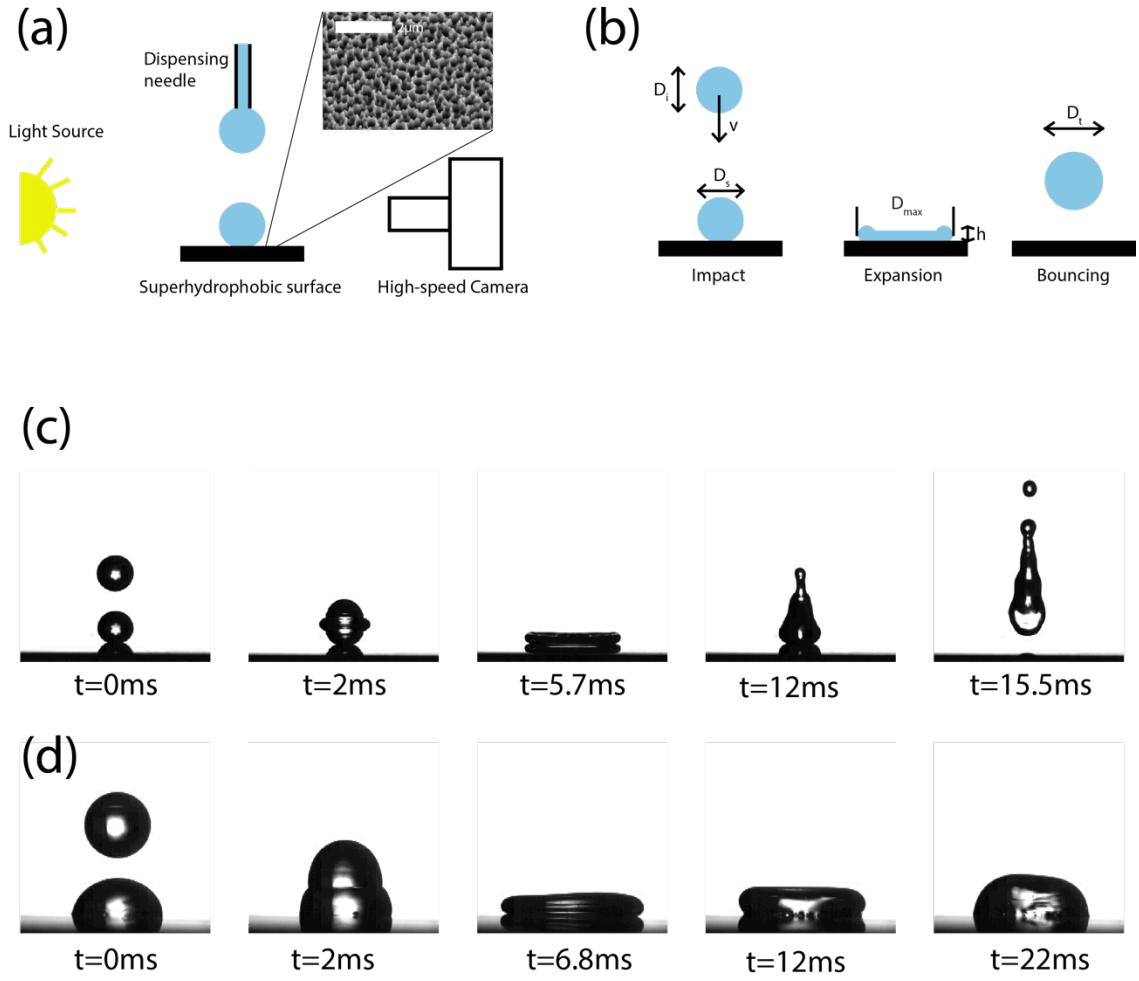

FIG. 1. (a) Schematic of the experimental setup. A high-speed camera films the impact of a droplet on a second droplet gently deposited on the surface. The surface is superhydrophobic and the SEM image in the inset shows the nanograss texture. (b) Schematic of the typical phases of drop-on-drop impacts: The droplets coalesce and expand until they reach a maximum diameter D_{max} corresponding to a thickness h, then retract and bounce off. (c-d) Snapshots of the high-speed video of drop-on-drop impacts.

(c) corresponds to the inertial-capillary regime ($D_i = D_s = 2.3mm\,, V = 1.10ms^{-1}, \mu = 8.9.10^{-4}Pa.s$ $(water)$), while (d) corresponds to the viscous regime ($D_i = D_s = 3.4mm\,, V = 1.23ms^{-1}, \mu = 0.34Pa.s$). Videos are available in [56].

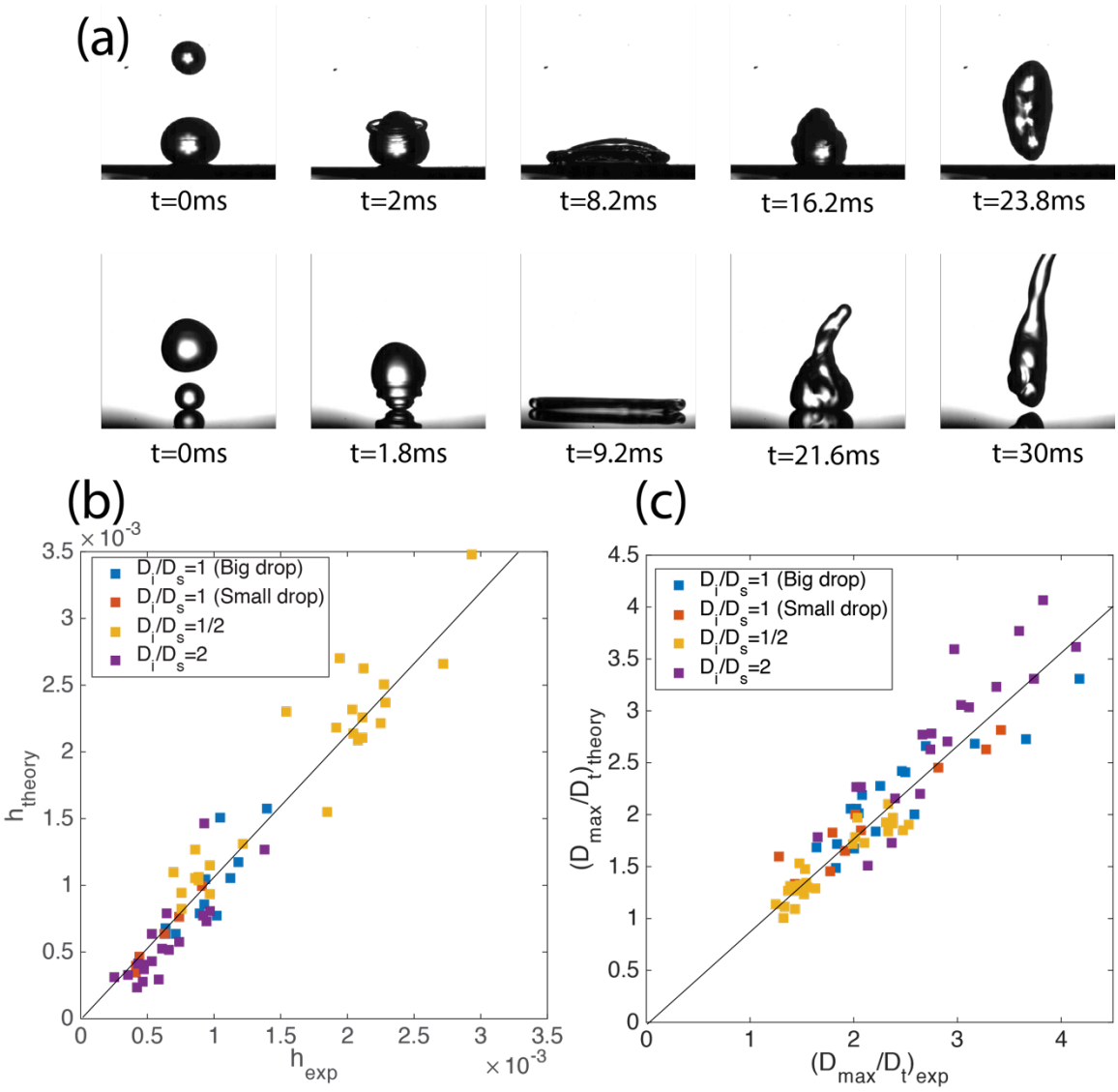

FIG. 2. (a) Snapshots of the high-speed video of the impact of small water droplet on a bigger one (first row: $D_i = 2.3mm\,, D_s = 3.5mm\,, V = 1.6ms^{-1}$) and vice-versa (second row: $D_i = 3.8mm\,, D_s = 2.0mm\,, V = 0.98ms^{-1}$). Both impacts are in the inertial-capillary regime. Videos are available in [56]. (b) Comparison of predicted (solid line)

droplet thickness at maximum expansion and experimentally measured (symbols) thicknesses for various drop size ratios, velocities and viscosities. The solid line is a linear fit (y=1.09x, R2=0.899). (c) Comparison of predicted and experimentally measured maximum diameter for the same data. The solid line is a linear fit (y=0.91x, R2=0.887).

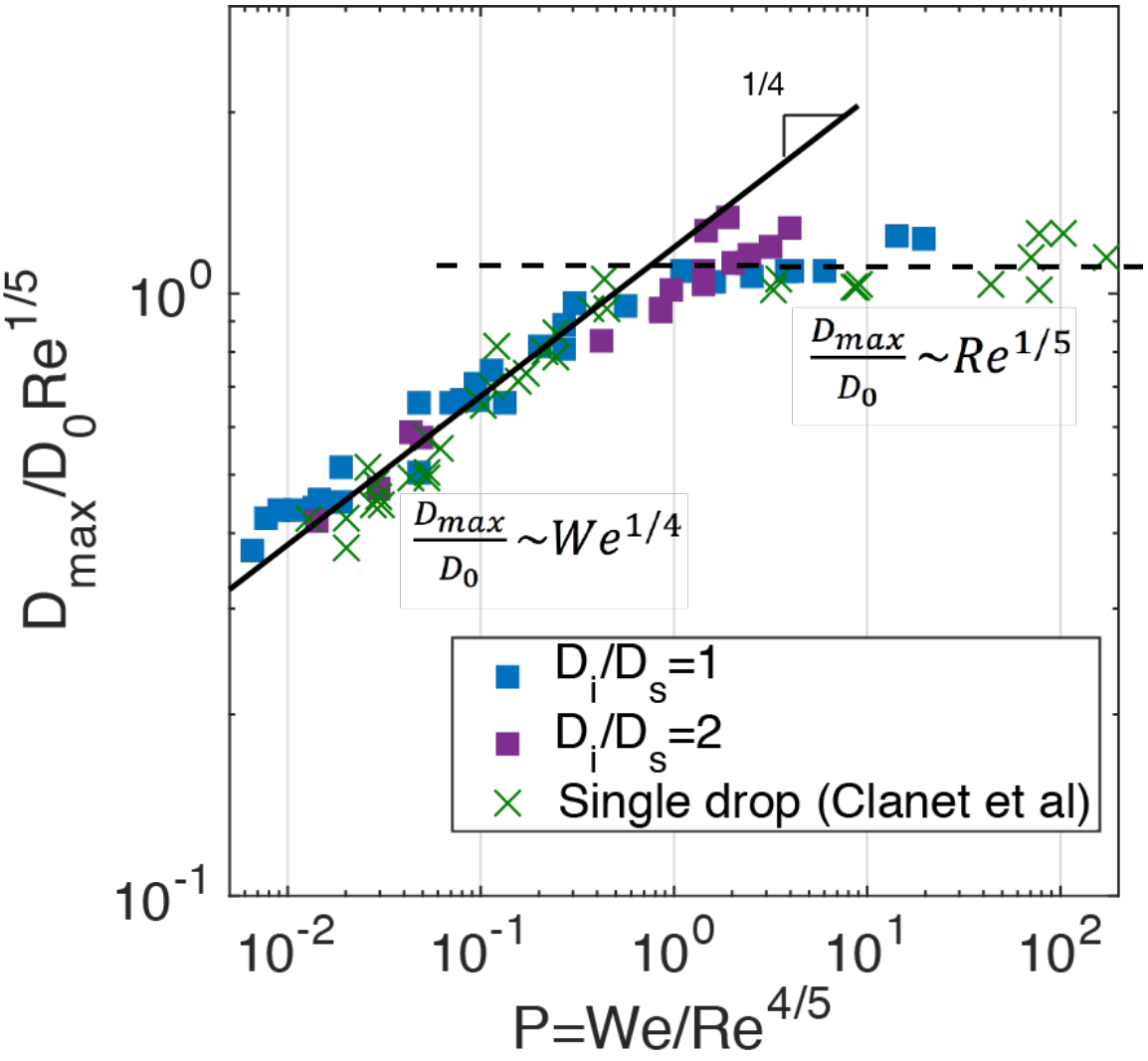

FIG. 3. Maximum expansion diameter results for drop-on-drop impacts. The x-axis is the Impact parameter P and the y-axis is the product of the normalized maximum diameter by the Reynolds number to the power 1/5. Two distinct regimes are observed. In the inertial-capillary regime ($P < 1$, solid line has a slope of 0.25 with a coefficient of determination R^2=0.897), $\frac{D_{max}}{D_t}$ varies as the $We^{1/4}$ and does not depend on viscosity. In the viscous

regime ($P < 1$, dashed line), $\frac{D_{max}}{D_t}$ varies as the $Re^{1/5}$. The shown data are our results for size ratios of 1 and 2 as well as single drop data from literature. All data collapse on a single master curve.

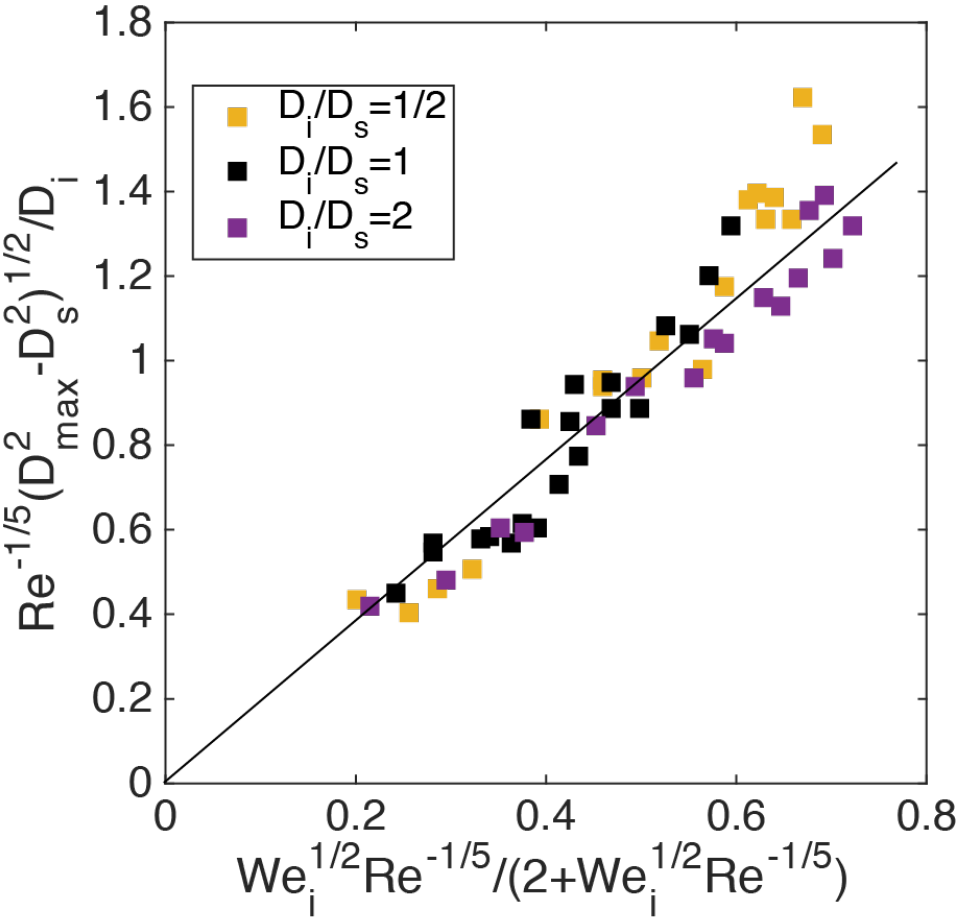

FIG. 4. Maximum expansion diameter results for drop-on-drop impacts with alternative model. The x-axis is the modified interpolation function from Laan et. al. and the y-axis is the product of the normalized maximum diameter by the Reynolds number to the power -1/5. The solid line is a linear fit (y=1.95x) with R2=0.898.

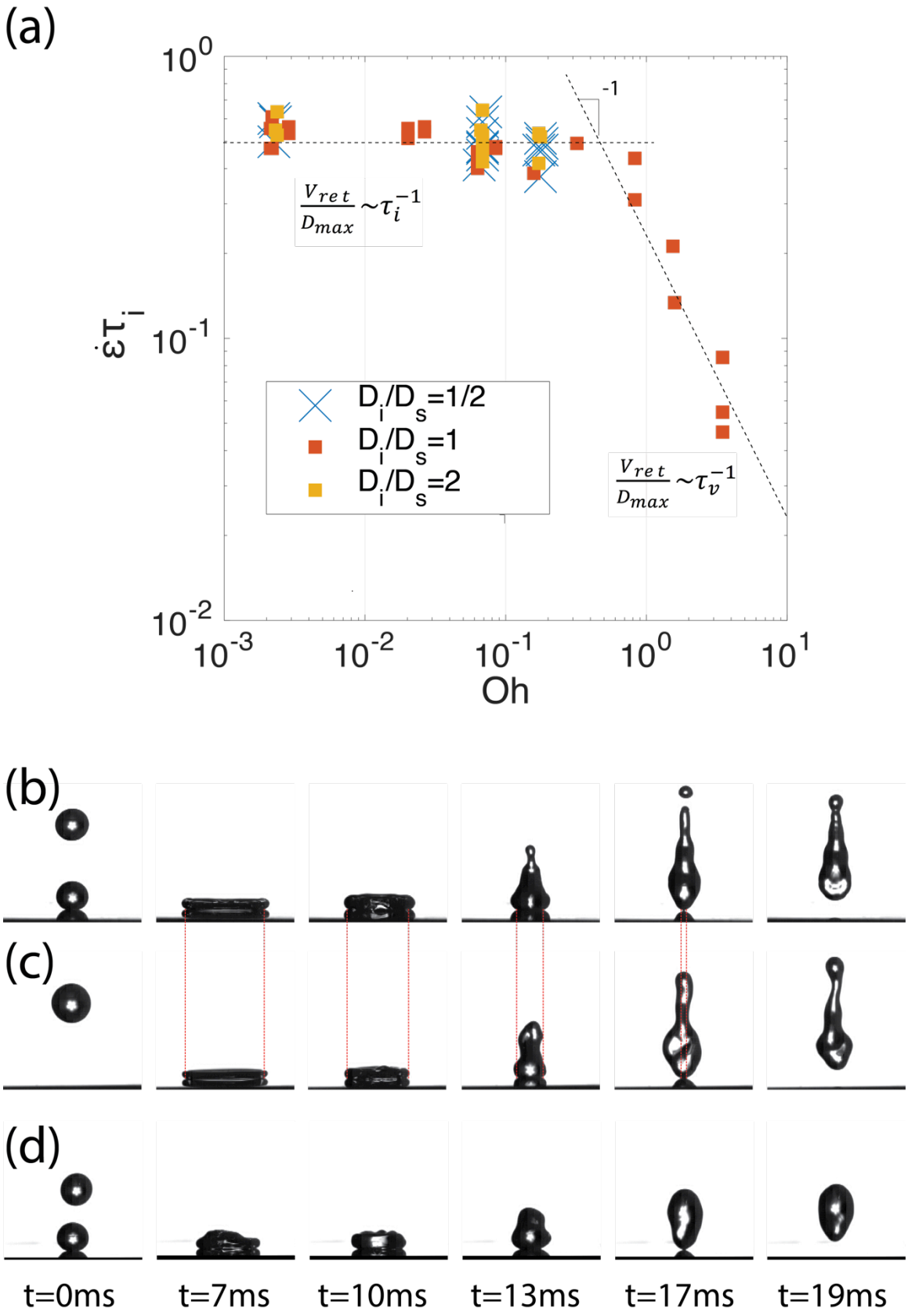
(a)
10^0
10^{-1}
10^{-2}
$\varepsilon \cdot \tau_i$
10^{-3}
10^{-2}
10^{-1}
10^0
10^1
Oh
-1
$\frac{V_{ret}}{D_{max}} \sim \tau_i^{-1}$
$\frac{V_{ret}}{D_{max}} \sim \tau_v^{-1}$
D_i/D_s=1/2
D_i/D_s=1
D_i/D_s=2
(b)
(c)
(d)
t=0ms
t=7ms
t=10ms
t=13ms
t=17ms
t=19ms

FIG. 5. (a) Retraction results for drop-on-drop impacts. The x-axis is the Ohnesorge number and the y-axis is the product of the retraction rate by the inertial-capillary timescale. Two distinct regimes are observed. In the inertial-capillary regime $\dot{\epsilon}\tau_i$ is constant and does not depend on impact velocity, viscosity and size ratio. In the viscous regime $Oh > 0.5$, the retraction rate scales as the inverse of the viscous-capillary timescale. (b) Snapshots of a drop-on-drop impact of water droplets of the same size ($D_i = D_s = 2.3mm\,, V = 1.25ms^{-1}$). (c) Snapshots of a single water drop impact ($D_i = 2.9mm\,, V = 0.98ms^{-1}$). The contact line moves exactly the same as the last case in the retraction phase. (d) Snapshots of a drop-on-drop impact of water droplets of the same size ($D_i = D_s = 2.3mm\,, V = 0.71ms^{-1}$). Videos are available in [56].